Journal of Applied Electrochemistry (2023) 53:2239–2248
https://doi.org/10.1007/s10800-023-01910-2

RESEARCH ARTICLE

Aptamer-based impedimetric label-free detection of bisphenol A from water samples using a gold nanoparticle-modified electrochemical nanofilm platform

Rukiye Saygılı-Canlıdinç[1] · Mustafa Oguzhan Caglayan[2] · İshak Afşin Kariper[3] · Zafer Üstündağ[1] · Samet Şahin[2]

Received: 2 January 2023 / Accepted: 25 April 2023 / Published online: 10 May 2023

Abstract

A label-free impedimetric aptasensor for bisphenol A (BPA) was developed based on a novel method. Initially, gold nanoparticle-based nanoplatforms were prepared using a 4-mercaptophenyl (4MP) electrochemical nanofilm. Then, the BPA-selective aptamer (antiBPA) was immobilized on this platform for the sensitive and selective detection of BPA. The characterizations of the electrode preparation steps were performed using a transmission electron microscope, X-ray photoelectron spectroscopy, electrochemical methods, and atomic force microscopy. The aptamer immobilization concentration, immobilization time, and incubation time of BPA were optimized to get the best sensor response. The calibration curve exhibited good linearity between 10 fM and 10 nM with a correlation coefficient of 0.9963 and a limit of detection and limit of quantification values of 8.6 and 25.8 fM (S/N = 3), respectively. The developed aptasensor showed good reproducibility (RSD 2.55%), high sensitivity, specificity, and stability. The developed sensor was validated using real samples of tap water, lake water, and wastewater demonstrating promising performance.

Graphical abstract

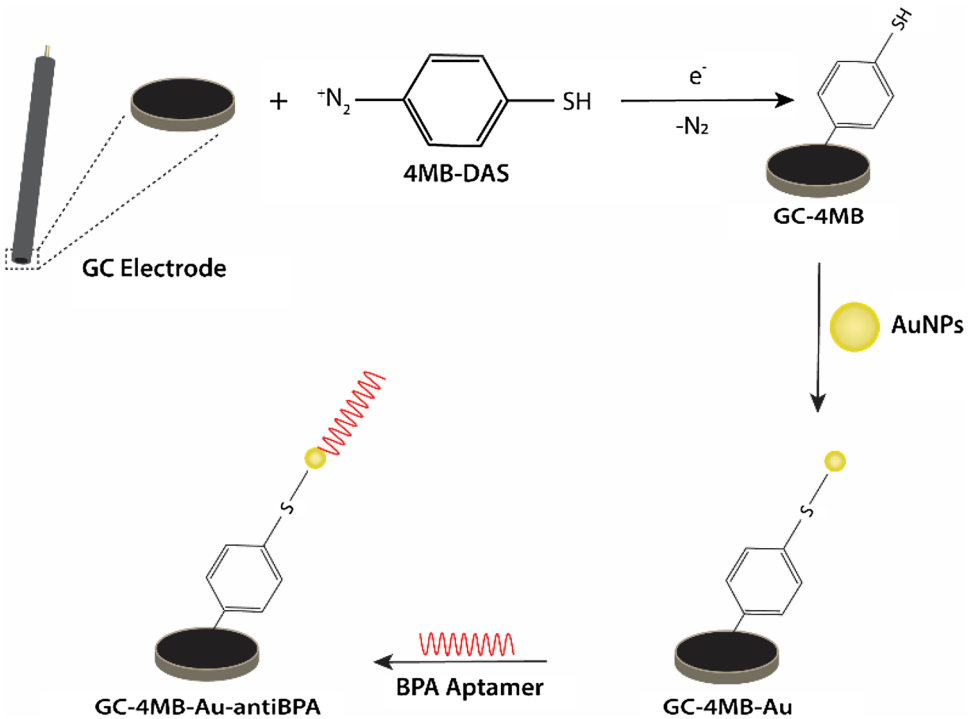

Keywords Gold nanoparticle · Bisphenol A · Aptamer · Sensor · Potentiostat/Galvanostat

Extended author information available on the last page of the article

1 Introduction

Environmental pollution has become one of the key problems for human health because of fast population growth and subsequent industrialization. Monitoring these pollutants in the appropriate environment is critical for pollution control. Methods for monitoring these pollutants can provide reliable and highly sensitive environmental sample analysis. However, they require expensive analytical equipment and experienced technicians, making them unsuitable for an on-site and quick examination. Therefore, developing a simple and effective analytical approach for detecting environmental contaminants is desirable [1].

Endocrine-disrupting chemicals (EDCs), heavy metals, phenols, poly-hydroxy biphenyls, dyes, pesticides, and pharmaceuticals can be listed as some examples of such contaminants [2, 3]. In recent years, there is a growing concern about EDCs that can affect the endocrine system and the metabolism of steroid hormones [4]. An increasing number of studies have reported the adverse effects of 800 different EDCs on human and wildlife health [5]. EDC exposure can cause obesity, diabetes, and cardiovascular diseases and increases the risk of cancer and neurotoxicity [6]. As a consequence, EDCs are defined by the US Environmental Protection Agency as exogenous and anthropogenic agents that have adverse effects on the environment and the human body [7].

Bisphenol A (BPA, 2,2-bis(4-hydroxyphenyl)propane) is one the hazardous EDCs that pose a threat to human health and wildlife even at low doses [1]. It is a non-biodegradable biological antioxidant and is widely utilized in polymeric materials as a plasticizer agent in the production of polyacrylates, polycarbonate plastics, polyester, pesticides, epoxy resins, and so on [8, 9]. BPA is commonly found in food and beverage containers, dental amalgams, water bottles, flame retardants, medical gadgets, children's toys, food packaging, and as well as many other plastic products in medical devices, automobiles, construction materials, electrical/electronic equipment, and small electronic devices [10]. Its presence in such commonly used materials increases the potential contamination risk of BPA [11]. Accordingly, BPA has become a common pollutant and has been reported in wastewater, river water, sediments, and raw sewage effluents at concentrations ranging from nM to µM [12, 13, 14, 15].

As with other EDCs, BPA's effects on the endocrine system, particularly reproductive abnormalities, occur as a result of BPA's binding to estrogen receptors [16]. It has been reported that BPA causes a decrease in sperm quality in humans [17, 18], and causes adverse effects such as reproductive disorders, neural disorders, chronic diseases, and the formation of various types of cancer in vitro animal models, even at low concentrations of BPA intake [19, 20]. In addition, these potentially dangerous effects of BPA on humans have been confirmed by relevant studies [21, 22]. After introducing strict regulations on the production and use of BPA, different derivatives have been produced and used as an alternative to BPA [23, 24, 25]. Rapid and sensitive detection methods were needed for the detection and monitoring of BPA and similar derivatives, whose maximum permissible levels were determined by taking them as pollutants for the many reasons mentioned previously. So far, numerous analysis techniques have been used for environmental monitoring, including spectroscopic, chromatographic, and electrochemical technologies [26]. These methods include but are not limited to, surface-enhanced Raman spectroscopy (SERS) [9], colorimetric methods [27], fluorescence spectroscopy [28], and HPLC [29]. Although many of these methods are highly sensitive and accurate when operated by professionals, they are expensive, time-consuming, cumbersome, and/or require sample pretreatment. In addition, the detection and monitoring of low molecular weight pollutants in water resources in situ and real-time is also limited due to the method applied where the analyzes are complicated.

Electrochemical techniques, on the other hand, have been very attractive in recent years since they are cheap, reliable, sensitive, and practical methods. Impedimetric electrochemical sensors are especially of great interest using different recognition elements such as antibodies and imprinted polymers [30, 31]. Recently, a review of the detection of BPA has been reported focusing on aptamer-based sensor platforms including electrochemical sensors [26]. Table S1 shows several reported electrochemical methods for BPA detection and their analytical performance parameter comparisons. In this study, a single-stranded (ss) DNA aptamer, as a BPA recognition element, which has inherent advantages compared to antibodies, was used. Aptamers can be used in many sensor platforms to detect environmental pollutants, food toxicants, and disease-related metabolites at the molecular level [32]. They are often selected from a random pool of ~ 10^{15} molecules until they have sufficiently high affinity, typically ranging from micro-molar (µM) to nano-molar (nM) or higher [33, 34, 35]. This high affinity enables aptamers to recognize their targets with high selectivity [36].

Herein, a bare glassy carbon (GC) electrode was modified with 4-mercaptophenyl nanofilm using an electrochemical reduction method of the diazonium salt. Then, Au nanoparticles (AuNPs) were attached to the thiol-terminated surface. The nanoparticle immobilized surface was modified with the BPA-specific aptamer (AntiBPA) as self-assembled monolayers. The BPA probe and its components were characterized by different techniques such as transmission electron microscope (TEM), X-ray photoelectron spectroscopy

(XPS), electrochemical methods, and atomic force microscopy (AFM). Optimization parameters of the probe were investigated as the AntiBPA concentration to be bound to the surface and the incubation time of the BPA. Then, the electrochemical impedance spectroscopy (EIS) technique was used to obtain the calibration curve for sensitive and selective BPA detection. The effect of the species likely to interfere with the BPA on the sensor response was investigated. The developed method was applied to detect BPA in lake water, tap water, and wastewater real samples.

2 Experimental

The chemicals used in the study were of HPLC purity and were obtained from the local representatives of chemical suppliers such as Merck, Riedel, and Sigma-Aldrich. Aptamers were obtained from the local representative of Molbiol (Germany), and each batch used was supplied as a lyophilized sample synthesized and purified at a 200 nmol scale. AntiBPA reported in the literature was used as SH-C_6H_{12} modified from the 5'-terminus for the study [37]. The sequences of the antiBPA and control aptamers used in this study are as follows (from 5′ to 3′); CCG GTG GGT GGT CAG GTG GGA TAG CGT TCC GCG TAT GGC CCA GCG CAT CAC GGG TTC GCA CCA, and CCG TCT TCC AGA CAA GAG TGC AGG G.

The pure water used is ultra-pure quality (UPW) water with a resistance of 18.3 MΩ cm (Human Power 1 + Scholar purification system). All Electrochemical measurements were performed at room temperature (25 ± 1 °C) using a PCI4/300 potentiostat/galvanostat (Gamry Instruments, PA, USA) with a BASi (USA) C3 Cell Stand. A three-electrode electrochemical cell was used for all electrochemical experiments. Reference and counter electrodes were used as an Ag/$AgCl_{sat}$ and platinum wire. A modified platform was prepared on a GC surface (BASi MF-2012, with a geometric area of 0.071 cm^2). Before the electrochemical experiments, the solutions were completely deoxygenated by purging with purified argon (99.99%) for 10 min. Aptamer solutions were prepared in phosphate buffer saline (PBS, 0.01 M Na^+, pH 7.4). Cyclic voltammetry (CV) experiments were performed at a scan rate of 200 mV/s with a step potential of 2 mV. Impedimetric measurements (EIS) were recorded between 0.01 Hz and 100 kHz at a sinusoidal voltage perturbation of 5 mV amplitude with a DC potential of 0.4 V. EIS data were fitted using equivalent circuit tools provided in Echem Analyst™ Software (Gamry Instruments, USA).

2.1 Electrode modification protocol with aptamer

The GC electrodes were polished with 1000 nm, 300 nm, and 50 nm aluminum oxide slurry on micro cloth pads (Buehler, USA). All GC electrodes were sonicated in the water twice and then in a 1:1 (v/v) isopropyl alcohol and acetonitrile (1:1, v/v) mixture for 10 min each [38]. Electrochemical diazonium salt modification was performed according to the literature [39]. 100 mg of 4-aminothiophenol was dissolved with 15 mL, 0.5 M HCl in a voltammetric cell in ice bathing. Ice-cold aqueous 200 mg of $NaNO_2$ solution was

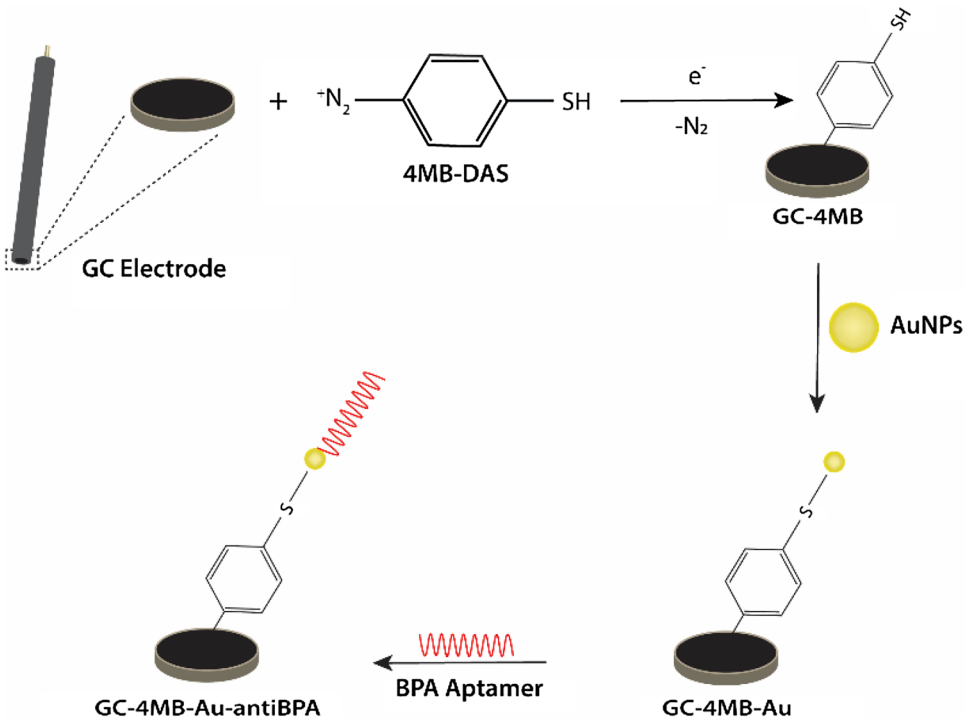

Fig. 1 Schematic representation of the preparation of the GC-4MP-Au-antiBPA electrode

added into the acidic solution drop by drop and stirred for 45 min keeping at 0 °C during the reaction. GC electrodes were then dipped into the 4-mercaptobenzene diazonium salt (4 MB-DAS) solution and diazonium salt modification was performed by CV. The modified surface was denoted as GC-4MP (4-mercaptophenyl modified glassy carbon).

AuNPs were prepared with the colloidal method, described elsewhere [40]. In brief, 20 mL 1.0 mM $HAuCl_4$ was added into a 100 mL volumetric flask on a stirring hot plate. During vigorous stirring, 2 mL of $Na_3C_6H_5O_7{\cdot}2H_2O$ (1%) was slowly added to the gold precursor solution at boiling temperature. The mixture was well mixed at the same temperature until the color of the solution changed to Bordeaux color, and then it was suddenly cooled. The mean diameters of the AuNPs are maximum of 35 nm and the AuNPs were stabilized with ethanol [41].

A schematic representation of the GC-4MP-Au-BPa electrode modification steps is given in Fig. 1. Briefly, AuNPs were attached on thiol-terminated GC-4MP surface for 2 h via self-assembly route, and this surface was denoted as GC-4MP-Au. Then, 10 µL of 2 µM antiBPA solution in PBS was dropped on the GC-4MP-Au surface for 2 h. The aptamer-modified surface (GC-4MP-Au-antiBPA) was washed with PBS followed by 1 mM 6-mercapto-1-hexanol (MCH) solution in PBS to block the unoccupied Au surface to minimize non-specific interactions. The antiBPA-modified electrodes were kept at 4 °C before use.

2.2 Characterization of the modified surface

GC-4MP-Au-antiBPA surface and its components were characterized using various methods including electrochemical methods CV and EIS, AFM (Park Systems, NX10, S. Korea), and XPS. The XPS measurement was carried out with a PHI 5000, Versa Probe—Φ ULVAC-PHI. Inc., Japan/USA) X-ray photoelectron spectrometer. AuNPs were characterized with a TEM (JEOL Ltd., Tokyo, Japan).

2.3 BPA measurements

Parameters such as the concentration of antiBPA and its incubation time were optimized before BPA measurements. The electroanalytical performance of the aptamer in the detection of BPA was evaluated using a solution of 10 nM–10 fM BPA in PBS. The limit of detection (LOD) and limit of quantification (LOQ) was calculated using the response of three times the standard deviation of zero-pose response (3σ) which was measured based on the standard deviation of the blank samples on the aptasensor

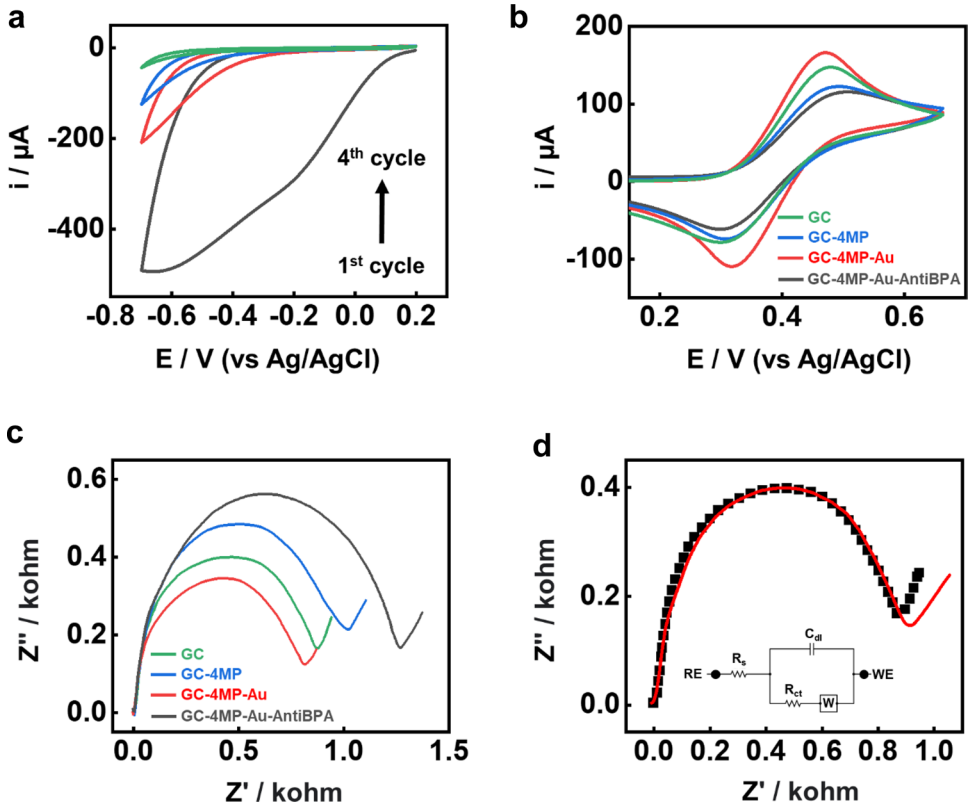

Fig. 2 **a** Modification voltammogram of 4-MB-DAS on a GC electrode in MeCN (0.5 HCl) vs. $Ag/AgCl_{sat}$, at a scan rate of 200 mV/s, **b** CVs and **c** Nyquist plots of 2 mM $K_4Fe(CN)_6$/$K_3Fe(CN)_6$ in 0.1 M KCl using GC, GC-4MP, GC-4MP-Au, and GC-4MP-Au-anti BPA electrodes, and **d** the fitted EIS data of GC electrode and the equivalent circuit (inset)

and LOQ is calculated using three times the LOD value. Selectivity studies were performed with possible interfering substances including bisphenol (BP), diethyl phthalate (DEP), resorcin (RES), and dibutyl phthalate (DBP). For the validation of the developed analytical strategy, precision and accuracy tests were also performed using two different BPA concentrations. The results were evaluated using inter-day and intra-day experiments. Finally, real samples from tap water, lake water, and wastewater were tested using the developed method. The lake water was obtained from two different artificial lakes on the Kütahya Dumlupınar University campus.

3 Results and discussions

3.1 Modification and characterization

Figure 2a shows the CVs obtained from the electrochemical reduction of 4 MB-DAS. The multicycle modification voltammogram of the electrochemical modification is very characteristic of the reduction of the 4 MB-DAS [42]. After the first cycle, the 4-mercaptophenyl (4MP) terminated groups were covalently attached to the carbon surface, while the peak current decreased drastically in subsequent cycles.

The typical behavior of the diazonium salt shows that an irreversible reduction took place resulting in the formation of a 4-MP radical covalently attached to the GC surface. Although the electrode modification took place at the first cycle, extra cycles were applied to coat surface pinholes with the 4MP. All modified surfaces (GC, GC-4MP, GC-4MP-Au, GC-4MP-Au-antiBPA) were characterized by CV and EIS techniques using a redox couple (2 mM $K_4Fe(CN)_6$/$K_3Fe(CN)_6$ in 0.1 M KCl). The CV and EIS characterization results are given in Fig. 2b and c, respectively.

In Fig. 2b, the anodic peak current of the redox couple on GC, GC-4MP, GC-4MP-Au, GC-4MP-Au-antiBPA were ca. 147 µA, 123 µA, 166 µA, and 122 µA, respectively. The GC electrode anodic peak decreased and the cathodic peak didn't differ upon diazonium salt modification as expected due to the multilayer formation of the 4-MP on the surface of the electrode hindering the electron transfer. It might be because the 4-MP thickness is greater than 5 nm which is not short enough for the quantum mechanical tunneling effect [43]. On the other hand, a significant increase in anodic and cathodic peaks was observed resulting in enhanced chemical and electrochemical reversibility after AuNP modification. This is due to the highly conductive nature of the AuNPs on the surface causing a more efficient electron transfer between the electrode and the redox probe [44, 45]. While electron transfer of the redox probe was very fast in GC-4MP-Au, a dramatic decrease occurred at the aptamer-bound surface. The surface coverage with the aptamer also caused electrochemical irreversibility as the peak separation increased by ca. 35 mV. Impedimetric measurement results in Fig. 2c were found to be very compatible with CV results. The charge transfer resistance of the redox couple on the aptamer terminated surface (GC-4MP-Au-antiBPA) has increased considerably. This is due to the increased surface coverage of the non-conductive ssDNA molecule, the antiBPA, adding extra resistance for the redox probe, hence higher impedance. This behavior of ssDNA probes is widely studied and similar results were shown in the literature for impedimetric aptasensors [46]. Figure 2d shows the fitted EIS data of the GC electrode and the equivalent circuit that was used in all impedimetric measurement analysis.

The TEM image of the synthesized AuNPs is given in Fig. 3a demonstrating that AuNPs have a maximum diameter of ca. 35 nm. GC-4MP-Au surface was also characterized by XPS and high-resolution narrow spectra of Au_{4f} and S_{2p} are given in Fig. 3b and c, respectively. The Au_{4f} doublet peaks located at 89.1 eV and 85.4 eV in the Au_{4f} narrow region are attributed to immobilized AuNPs via self-assembly modification. The S_{2p} region corresponding to the spin–orbit coupling has also been characterized. The binding energy of $S_{2p1/2}$ and $S_{2p3/2}$ doublet peaks was calculated as 167.9 eV and 163.3 eV, respectively. These peaks correspond to the binding of sulfur to the surface, which is evidence of bonding between the thiol end-group of aptamers and the Au electrode surface. The AFM images of GC and GC-4MP-Au-antiBPA surfaces are also shown in Fig. 3d and e, respectively. The root-mean-square (RMS) roughness values of the bare GC and GC-4MP-Au-antiBPA were calculated as 1.79 nm and 31.7 nm, respectively. Considering AuNP included aptamer on the GC surface and bare GC, the calculated values are consistent with the surface morphology indicating a more rough surface for an antiBPA-modified electrode.

3.2 Optimization and calibration

Before the BPA analysis with the GC-4MP-Au-antiBPA electrode, two different parameters were first optimized. The optimum concentration of aptamer (AntiBPA) to be immobilized on the GC-4MP-Au electrode surface was first determined. The sensor response of 10 nM BPA in PBS was recorded after immobilizing antiBPA at different concentrations (0.5, 1, 1.5, 2, 2.5, and 3 µM antiBPA in 0.01 M PBS) on the GC-4MP-Au electrode surfaces for 2 h. Nyquist plots of 2 mM $K_4Fe(CN)_6$/$K_3Fe(CN)_6$ in 0.1 M KCl were obtained for the prepared electrode surfaces and the sensor working principle is shown in Fig. 4a. In the absence of the antiBPA, a faster and more efficient electron transfer can be obtained due to a less blocked surface, however, upon incubation with antiBPA, slower electron kinetics and higher charge transfer resistance can be

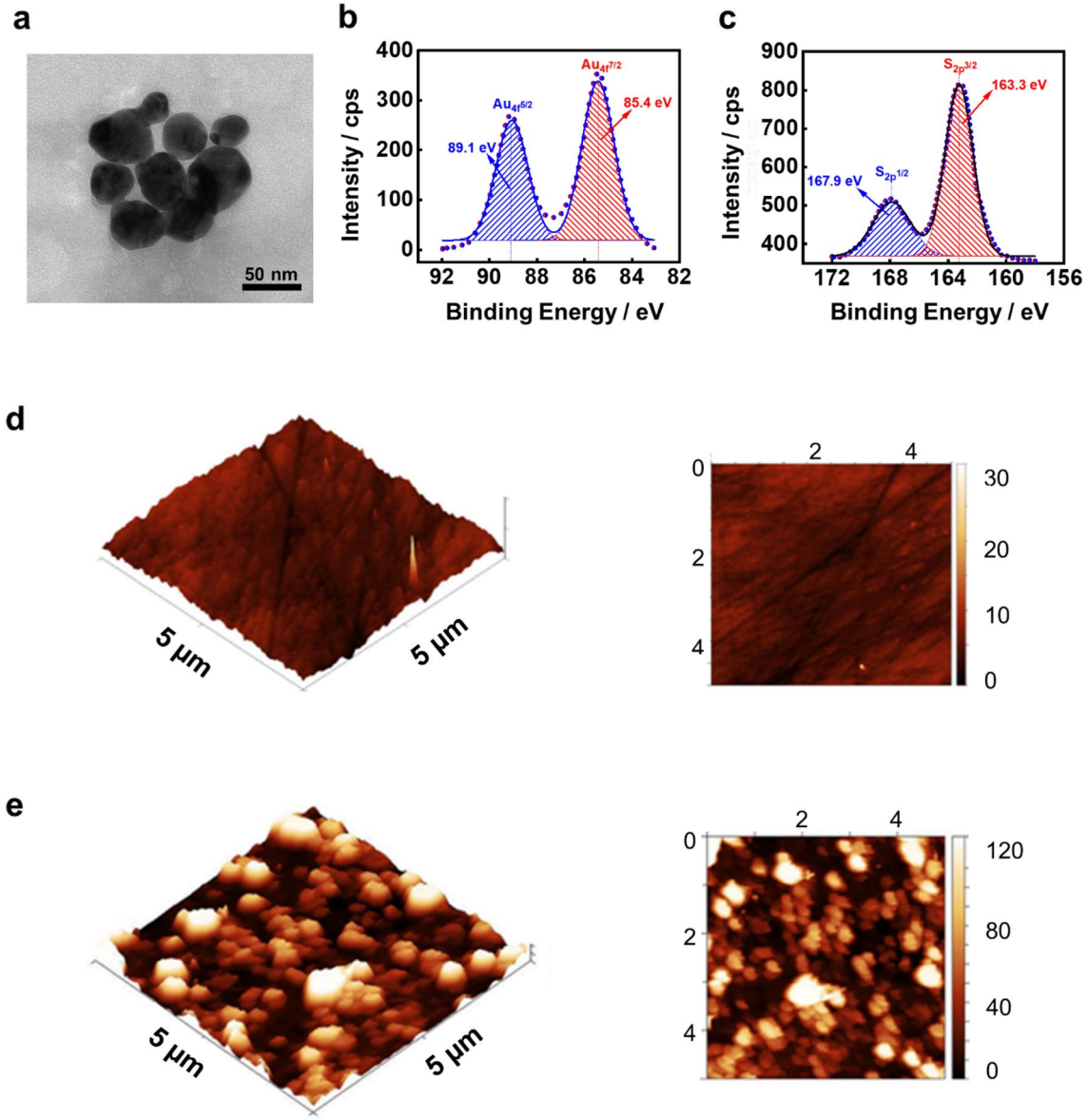

Fig. 3 **a** TEM image of the AuNPs, high-resolution X-ray photoelectron spectra of **b** Au_{4f} and **c** S_{2p} of GC-4MP-Au, AFM images of **d** bare GC electrode, and **e** GC-4MP-Au-antiBPA electrode

observed due to surface blockage. Since the charge transfer resistance didn't change after two consecutive antiBPA concentrations, the optimum concentration at which the resistance of the redox probe is maximum was determined as 2 µM (Fig. 4b).

The second optimization parameter was the aptamer (antiBPA) immobilization time on GC-4MP-Au electrode. Immobilization durations using 2 µM antiBPA were selected as 0.5, 1, 1.5, 2, 2.5, and 3 h to ensure an optimum degree of immobilization on the surface has been achieved. Figure 4c shows the Nyquist plots for the selected immobilization times and the optimum value was selected as 2 h since the response didn't change for the latter durations. Finally, the incubation time of the BPA solution was optimized on the surface of the GC-4MP-Au-antiBPA which is prepared using a 2 µM antiBPA during the immobilization. The Nyquist plots were obtained using 2 mM $K_4Fe(CN)_6/K_3Fe(CN)_6$ in 0.1 M KCl on GC-4MP-Au-antiBPA electrodes after the incubation of 10 nM BPA for different incubation times (0.5, 1, 2, 3 h) are given in Fig. 4d. The optimum incubation time to obtain the maximum signal of the 10 nM BPA solution was 2 h after obtaining a stable resistance value indicating a saturated surface response.

The calibration curve was obtained for BPA at different concentrations using the GC-4MP-Au-antiBPA electrode surfaces prepared according to the optimum conditions.

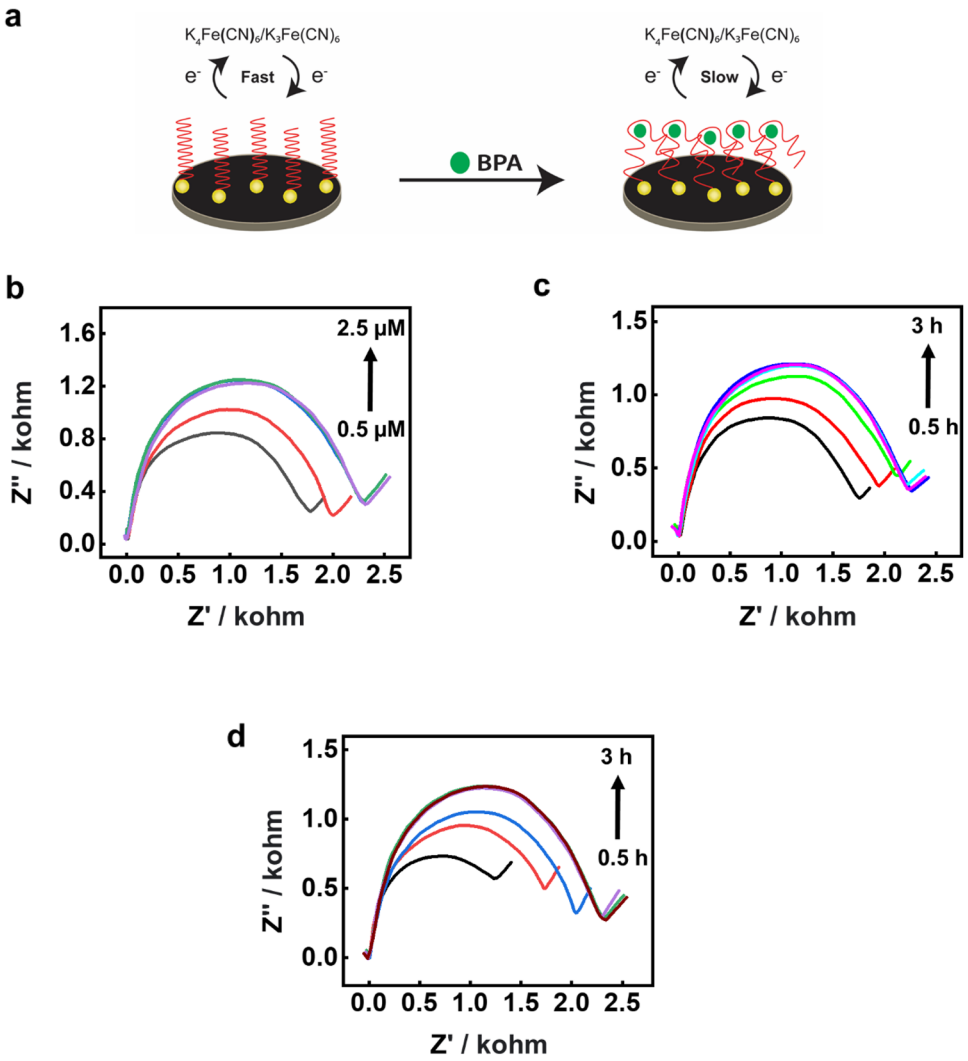

Fig. 4 **a** Schematic representation of the sensor detection strategy, Nyquist plots of 2 mM $K_4Fe(CN)_6/K_3Fe(CN)_6$ in 0.1 M KCl immobilized at different **b** antiBPA concentrations on GC-4MP-Au electrode, **c** antiBPA immobilization time on GC-4MP-Au electrode, and **d** 10 nM BPA incubation times on GC-4MP-Au-antiBPA electrodes

Figure 5a shows Nyquist plots of the redox probe on the surface of GC-4MP-Au-antiBPA incubated with different concentrations (10 fM to 10 nM) of BPA. The calibration curve plotted using BPA concentration changes versus charge transfer resistances of the redox couple with different BPA concentrations is given in Fig. 5b.

The relative impedance shift (%) is calculated using $(R_{ct} - R_{ct0})/R_{ct0}$, where R_{ct0} is the initial impedance without BPA and R_{ct} is the impedance of the after incubation with different concentrations of BPA. Furthermore, the sensor also has good reproducibility with a maximum relative standard deviation of 2.55% for 5 individual sensor responses. Table 1 summarizes the calculated electroanalytical performance parameters of the developed sensor.

3.3 Precision and accuracy

The precision and accuracy tests of the developed sensor were done both using intra-day tests for seven consecutive days and inter-day precision tests for 5 independent samples using 1 pM and 10.0 nM BPA solution. Table S2 shows inter- and intra-day test results. The accuracy as relative error (RE) % of methods for inter-day and intra-day measurements was between −4.0% and +4.0%. Furthermore, the method's precision for inter-day and intra-day measurements was between 1.36 and 3.85%. Both results reveal quite good analytical performance in terms of the precision and accuracy of the method.

3.4 Selectivity and real sample analysis

The selectivity of the sensor in the presence of 1.0 nM BP, DEP, RES, and DBP solutions in PBS likely to interfere with 1.0 pM BPA was investigated. The selectivity results are given in Fig. 5c as a bar graph of relative impedance responses of BPA-aptasensor incubated with these species. The results show that the signal deviation of BPA does not change greater than 4.5%. The results show also that this

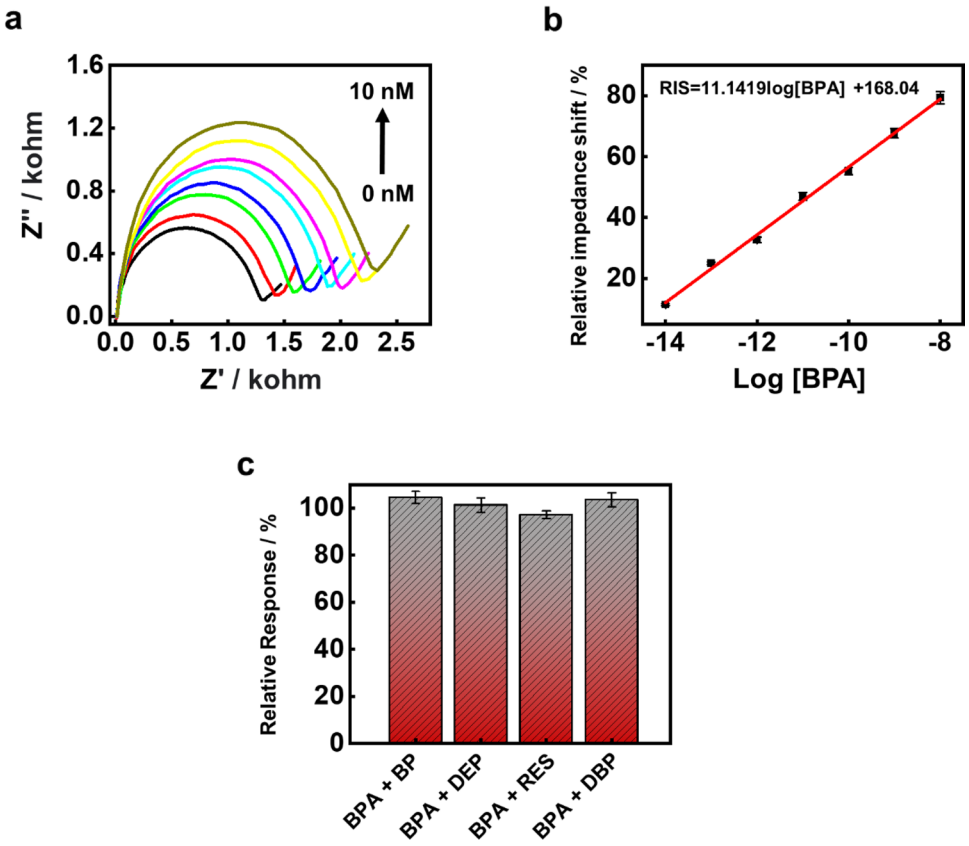

Fig. 5 **a** Nyquist plots obtained using 2 mM $K_4Fe(CN)_6$/$K_3Fe(CN)_6$ in 0.1 M KCl on the surface of GC-4MP-Au-antiBPA incubated with different concentrations (10 fM to 10 nM) of BPA, **b** the calibration curve of BPA detection, and **c** relative response change using BP, DEP, RES, and DBP

Table 1 Electroanalytical performance results of the developed method

Analytical parameters	Results
Linear concentration range, M	1×10^{-14}-1×10^{-8}
Linear equation	RIS = 11.1419 log[BPA] + 168.04
Standard error of the slope, ±	0.27
Standard error of the intercept, ±	3.0
R^2	0.9963
LOD, fM (S/N = 3)	8.6
LOQ, fM	25.8

signal deviation was not remarkable for 1 pM BPA with the 1000-fold concentrated interferents.

The developed sensor was also employed to detect spiked BPA amounts in various real samples consisting of lake water, tap water, and wastewater. The recovery ($n = 6$) values were determined using the spike method, and generally satisfactory results were obtained in terms of practical applications. Recoveries of BPA with varying concentrations added in lake water, tap water, and wastewater are given in Table 2.

Table 2 Recoveries of BPA with varying concentrations added in lake water, tap water, and, wastewater

Samples	Added BPA, pM	Detected, pM	Recovery, %
Lake water 1	–	ND	–
	10	9.78	97.8
	50	52.3	104.6
Lake water 2	–	ND	–
	10	10.38	103.8
	50	53.1	106.2
Tap water	–	ND	–
	10	9.96	99.6
	50	48.7	97.4
Wastewater	–	18.6	–
	10	27.3	95.4
	50	63.2	92.1

ND not detected

4 Conclusion

This study aims to develop a novel sensitive electrochemical BPA sensor using an aptamer-based GC-4MP-Au-antiBPA electrode. The electrode surface and electrode modification steps were characterized with electroanalytical (CV and EIS), spectroscopic (XPS), and microscopic (TEM and AFMs) techniques. Optimization of the concentration of aptamer loading for surface immobilization and incubation time of the analyte were performed for the best sensor response. The calibration of the sensor has been obtained at the concentration range between 10 fM to 10 nM with LOD and LOQ values of 8.6 and 25.8 fM, respectively. The developed sensor platform showed satisfactory analytical performance compared to similar electrochemical sensor platforms for BPA detection. The selectivity against selected species (BP, DEP, RES, and DBP solutions), precision (between 1.36% and 3.85%), and accuracy (between − 4.0% and + 4.0%) of this proposed sensor platform are quite remarkable. Real sample tests also demonstrated the successful practical application potential of the developed sensor platform for BPA detection in water samples. Hence, this study could pave the way forward for the easy, low-cost, and sensitive detection of BPA in real samples.

Supplementary Information The online version contains supplementary material available at https://doi.org/10.1007/s10800-023-01910-2.

Acknowledgements The authors state no conflict of interest.

Author contributions RS-C: Conceptualization, Methodology, Investigation, Data Curation, Writing-Original draft preparation. MOC: Methodology, Investigation, Data Curation, Writing-Original draft preparation, Writing—Reviewing and editing draft preparation. İAK: Data Curation, Visualization, Writing- Original draft preparation. ZÜ: Conceptualization, Methodology, Investigation, Data Curation, Writing-Original draft preparation, Writing- Reviewing and editing draft preparation. SŞ: Methodology, Investigation, Data Curation, Writing-Original draft preparation, Writing- Reviewing and editing draft preparation, Writing the final manuscript version.

Declarations

Competing interests The authors declare no competing interests.

References

1. Zhao S et al (2022) A novel electrochemical biosensor for bisphenol A detection based on engineered *Escherichia coli* cells with a surface-display of tyrosinase. Sens Actuators B Chem 353:131063
2. Husain Q, Qayyum S (2013) Biological and enzymatic treatment of bisphenol A and other endocrine disrupting compounds: a review. Crit Rev Biotechnol 33(3):260–292
3. Al Sharabati M et al (2021) Biodegradable polymers and their nano-composites for the removal of endocrine-disrupting chemicals (EDCs) from wastewater: a review. Environ Res 202:111694
4. Zhang S et al (2020) Nanocomposites consisting of nanoporous platinum-silicon and graphene for electrochemical determination of bisphenol A. Microchim Acta 187(4):241
5. Plahuta M et al (2017) Toxic and endocrine disrupting effects of wastewater treatment plant influents and effluents on a freshwater isopod Asellus aquaticus (Isopoda, Crustacea). Chemosphere 174:342–353
6. Sofen LE, Furst AL (2020) Perspective: electrochemical sensors to monitor endocrine disrupting pollutants. J Electrochem Soc 167(3):037524
7. Kumar S, Datta D (2022) Separation of bisphenol-A using amberlite-1180 impregnated with tri-n-octylamine. Chem Data Collect 37:100815
8. Ji G et al (2022) A systematic comparison of the developmental vascular toxicity of bisphenol A and its alternatives in vivo and in vitro. Chemosphere 291:132936
9. Zhang X et al (2022) Measurement of trace bisphenol A in drinking water with combination of immunochromatographic detection technology and SERS method. Spectrochim Acta Part A Mol Biomol Spectrosc 267:120519
10. Kim JI et al (2022) Association of bisphenol A, bisphenol F, and bisphenol S with ADHD symptoms in children. Environ Int 161:107093
11. Dhanjai et al (2018) Advances in sensing and biosensing of bisphenols: a review. Anal Chim Acta 998:1–27
12. Fürhacker M, Scharf S, Weber H (2000) Bisphenol A: emissions from point sources. Chemosphere 41(5):751–756
13. Bolz U, Hagenmaier H, Körner W (2001) Phenolic xenoestrogens in surface water, sediments, and sewage sludge from Baden-Württemberg, south-west Germany. Environ Pollut 115(2):291–301
14. Heemken OP et al (2001) The occurrence of xenoestrogens in the Elbe river and the North Sea. Chemosphere 45(3):245–259
15. Fromme H et al (2002) Occurrence of phthalates and bisphenol A and F in the environment. Water Res 36(6):1429–1438
16. Segner H et al (2003) Identification of endocrine-disrupting effects in aquatic vertebrates and invertebrates: report from the European IDEA project. Ecotoxicol Environ Saf 54(3):302–314
17. Toppari J et al (1996) Male reproductive health and environmental xenoestrogens. Environ Health Perspect 104(suppl 4):741–803
18. Vandenberg LN et al (2007) Human exposure to bisphenol A (BPA). Reprod Toxicol 24(2):139–177
19. Huo X et al (2015) Bisphenol-A and female infertility: a possible role of gene-environment interactions. Int J Environ Res Public Health 12:11101–11116. https://doi.org/10.3390/ijerph120911101
20. Oppeneer SJ, Robien K (2014) Bisphenol A exposure and associations with obesity among adults: a critical review. Public Health Nutr 18(10):1847–1863
21. Chen S et al (2017) Rapid analysis of bisphenol A and its analogues in food packaging products by paper spray ionization mass spectrometry. J Agric Food Chem 65(23):4859–4865
22. Idowu GA, David TL, Idowu AM (2022) Polycarbonate plastic monomer (bisphenol-A) as emerging contaminant in Nigeria: levels in selected rivers, sediments, well waters and dumpsites. Mar Pollut Bull 176:113444
23. Peng Y, Wang J, Wu C (2019) Determination of endocrine disruption potential of bisphenol A alternatives in food contact materials using in vitro assays: state of the art and future challenges. J Agric Food Chem 67(46):12613–12625
24. Wang X et al (2014) Electrochemical determination of estrogenic compound bisphenol F in food packaging using carboxyl functionalized multi-walled carbon nanotubes modified glassy carbon electrode. Food Chem 157:464–469
25. Yang J et al (2014) Simultaneous determination of endocrine disrupting compounds bisphenol F and bisphenol AF using

carboxyl functionalized multi-walled carbon nanotubes modified electrode. Talanta 130:207–212
26. Caglayan MO, Şahin S, Üstündağ Z (2022) An overview of aptamer-based sensor platforms for the detection of bisphenol-A. Crit Rev Anal Chem. https://doi.org/10.1080/10408347.2022.2113359
27. Zhang D et al (2016) Colorimetric detection of bisphenol A based on unmodified aptamer and cationic polymer aggregated gold nanoparticles. Anal Biochem 499:51–56
28. Xu Z et al (2020) Aptamer-enhanced fluorescence determination of bisphenol A after magnetic solid-phase extraction using Fe3O4@SiO2@aptamer. Anal Methods 12(36):4479–4486
29. Su Y et al (2018) Extraction and detection of bisphenol A in human serum and urine by aptamer-functionalized magnetic nanoparticles. Anal Bioanal Chem 410(7):1885–1891
30. Garyfallou G-Z et al (2017) Electrochemical detection of plasma immunoglobulin as a biomarker for Alzheimer's disease. Sensors 17(11):2464
31. Işık D et al (2021) Electrochemical impedimetric detection of kanamycin using molecular imprinting for food safety. Microchem J 160:105713
32. Fukata H et al (2006) Comparison of Elisa- and LC-MS-based methodologies for the exposure assessment of bisphenol A. Toxicol Mech Methods 16(8):427–430
33. Geiger A et al (1996) RNA aptamers that bind l-arginine with sub-micromolar dissociation constants and high enantioselectivity. Nucleic Acids Res 24(6):1029–1036
34. Gold L et al (1997) From oligonucleotide shapes to genomic SELEX: novel biological regulatory loops. Proc Natl Acad Sci USA 94(1):59–64
35. Tuerk C, Gold L (1990) Systematic evolution of ligands by exponential enrichment: RNA ligands to bacteriophage T4 DNA polymerase. Science 249(4968):505–510
36. Jenison RD et al (1994) High-resolution molecular discrimination by RNA. Science 263(5152):1425–1429
37. Beiranvand ZS et al (2017) Aptamer-based electrochemical biosensor by using Au-Pt nanoparticles, carbon nanotubes and acriflavine platform. Anal Biochem 518:35–45
38. Erkal A et al (2015) An electrochemical application of MnO_2 decorated graphene supported glassy carbon ultrasensitive electrode: Pb2+ and Cd2+ analysis of seawater samples. J Electrochem Soc 162(4):H213
39. Morita K, Yamaguchi A, Teramae N (2004) Electrochemical modification of benzo-15-crown-5 ether on a glassy carbon electrode for alkali metal cation recognition. J Electroanal Chem 563(2):249–255
40. Huang H, Yang X (2003) Chitosan mediated assembly of gold nanoparticles multilayer. Colloids Surf A 226(1):77–86
41. Nguyen DT et al (2010) Experimental measurements of gold nanoparticle nucleation and growth by citrate reduction of HAuCl4. Adv Powder Technol 21(2):111–118
42. Üstündağ Z, Solak AO (2009) EDTA modified glassy carbon electrode: Preparation and characterization. Electrochim Acta 54(26):6426–6432
43. Sayed SY et al (2012) Charge transport in molecular electronic junctions: compression of the molecular tunnel barrier in the strong coupling regime. Proc Natl Acad Sci 109(29):11498–11503
44. Roushani M, Shahdost-Fard F (2019) Applicability of AuNPs@N-GQDs nanocomposite in the modeling of the amplified electrochemical Ibuprofen aptasensing assay by monitoring of riboflavin. Bioelectrochemistry 126:38–47
45. Shahdost-fard F, Roushani M (2017) Impedimetric detection of trinitrotoluene by using a glassy carbon electrode modified with a gold nanoparticle@ fullerene composite and an aptamer-imprinted polydopamine. Microchim Acta 184:3997–4006
46. Bogomolova A et al (2009) Challenges of electrochemical impedance spectroscopy in protein biosensing. Anal Chem 81(10):3944–3949

Authors and Affiliations

Rukiye Saygılı-Canlıdinç[1] · Mustafa Oguzhan Caglayan[2] · İshak Afşin Kariper[3] · Zafer Üstündağ[1] · Samet Şahin[2]

✉ İshak Afşin Kariper
akariper@gmail.com

✉ Samet Şahin
samet.sahin@bilecik.edu.tr

[1] Chemistry Department, Kütahya Dumlupınar University, 43100 Kutahya, Turkey

[2] Department of Bioengineering, Faculty of Engineering, Bilecik Seyh Edebali University, 11100 Bilecik, Turkey

[3] Faculty of Education, Erciyes University, 38039 Kayseri, Turkey